in Terahertz for Military and Security Applications IV, edited by D.L. Woolard, and R.J. Hwu, M.J. Rosker, J.O. Jensen, Proc SPIE 6212-06-1

Terahertz gain on inter-valence-band transitions in multilayer delta-doped p-GaAs structures

M. V. Dolguikh,[a] A.V. Muravjov,[a] R. E. Peale,[a] D. Bliss,[b] C. Lynch,[b] D. W. Weyburne[b] and W. R. Buchwald[b]

[a] Dept. of Physics, University of Central Florida, Orlando FL, 32816-2385
[b] Sensors Directorate, Air Force Research Lab., Hanscom AFB, MA 01731

ABSTRACT

A concept for a terahertz laser in vapor-phase-grown homoepitaxial GaAs with spatially periodic doping profile was theoretically explored. Monte Carlo simulation of hole transport in multilayer delta-doped p-GaAs/GaAs structures in crossed electric and magnetic fields was performed to investigate possibilities of the terahertz amplification on inter-valence-band light-to-heavy hole transitions. The results are compared to those calculated for uniformly doped bulk p-GaAs and recently proposed p-Ge/Ge structures. The improvement in the gain for delta-doped p-GaAs structures is about ~ 2 – 3 times over bulk p-GaAs. Terahertz laser generation in the considered GaAs device concept appears feasible, as is growth of structures with active thicknesses sufficient to support quasioptical cavity solutions at 100 μm vacuum wavelengths. Potential applications for the considered laser device include sensing of chem/bio agents and explosives, biomedical imaging, non-destructive testing, and communications.

Keywords: terahertz, far infrared, laser, germanium, silicon, gallium arsenide, epitaxy.

1. INTRODUCTION

The THz region of the electromagnetic spectrum, loosely defined here to span the range 0.3 to 20 THz, is of particular interest to various department of defence agencies. Imaging through dust, or so called "brown-out" conditions, as well as through fog, are of particular interest to both the Army and the Air Force for various tactical reasons. In such cases there is always a tradeoff between radiation loss and resolution. Longer, mm-waves have low loss but poor resolving power, while shorter, IR waves produce highly resolved images but with extremely poor penetration depth. This problem of loss versus resolution motivates investigations into the lower end of the above mentioned spectral range with the added constraint that any such system must also be portable in order to be of use in the field. The mid-THz range would show increased resolution when used in an imaging system but because of the increased loss is more suitable for use in well controlled environments such as personnel/package, and non-destructive industrial screening, as well as non-evasive medical imaging. Beyond imaging systems, the Air Force is interested in the mid- to upper-end of the THz spectrum for use in advanced threat warning systems, where biological and chemical agents have rich spectra, as well as remote earth sensing, and flame/plasma characterization.

Based on the above needs, a great interest has arisen in developing compact, portable, THz sources. At present, because the THz spectrum constitutes a gap between well-developed electronic and photonic source technology, both electronic and photonic approaches have been extended to produce THz radiation. Frequency multiplied electronic sources have demonstrated 3 mW of 1.9 THz radiation with just 0.2% conversion efficiency,[1] while quantum cascade lasers have demonstrated 4 mW of continuous-wave radiation at 4.4 THz with 33% efficiency at an operating temperature[2] of 48 K. Non-linear optical techniques, such as optical recification (OR) have also be used for THz generation. Although chromatic dispersion effects in a highly non-linear crystals such as GaAs, have historically limited the use of this material in OR based systems, quasi-phase-matching has recently been used to counter dispersion effects and produce THz radiation.[3] In Ref. 3, quasi-phase-matching was achieved through the growth of thick GaAs layers via hydride

vapor phase epitaxy (HVPE) on orientation-patterned substrates.[4] The development of the HVPE technique, capable of produce epilayers of GaAs 100s of microns thick, along with the potential to delta-dope this material p-type, motivates the investigation of this material for use as a THz gain medium utilizing inter-valence-band (IVB) effects in a fashion similar to what has recently been proposed for p-Ge/Ge structures.[5,6]

As previously stated, GaAs is a potential active medium for inter-valence-band (IVB) hot-hole THz lasers.[7-9] Monte Carlo simulations have shown that bulk uniformily-doped GaAs should have acceptable performance.[10] However, due to doubled (see below) impurity scattering rate (a consequence of lower dielectric constant) in GaAs relative to Ge, THz gain in p-GaAs devices is expected to be lower than in the well-established p-Ge lasers. Compared with Ge, GaAs has additional factors of polar optical phonon and acoustic piezoelectric phonon scattering processes. The latter is usually unimportant, but the polar optical phonon scattering has a significant role. Monte Carlo simulation results for GaAs illustrate these features.

For the IVB mechanism, the inverted population grows at certain ratios of applied, crossed, electric- and magnetic-fields, when light holes are accumulated on closed trajectories below the optical phonon energy, while heavy holes undergo rapid optical phonon scattering. Fig. 1 is a schematic quasiclassical explanation of the IVB laser mechanism that is valid at low applied fields where Landau-level spacing is much less than carrier kinetic energy. The emission of polar (circle) and non-polar (starburst) optical phonons is indicated. Polar optical-phonon scattering in III-V compounds[11] provides a "hard ceiling" for hot holes. Most of the scattering events occur right beyond the optical phonon threshold, which is 35 meV for GaAs.[12] In contrast, in non-polar semiconductors (Ge, Si) the optical-phonon emission rate grows slowly with energy from the threshold value. Light-hole life time, which is responsible for the inversion population and for the gain, is determined by acoustic phonon scattering, ionized impurity scattering, and carrier-carrier interaction. This limits the operation of the IVB hot-hole laser, which has been experimentally realized only for p-Ge, to low temperatures ($T < 20$ K) and low carrier concentration ($p \sim 10^{14}$ cm^{-3}).[7-9] The IVB amplification mechanism illustrated in Fig. 1 provides wide tunability of p-type hot-hole devices in the terahertz frequency range (1.5 – 4.2 THz for p-Ge).

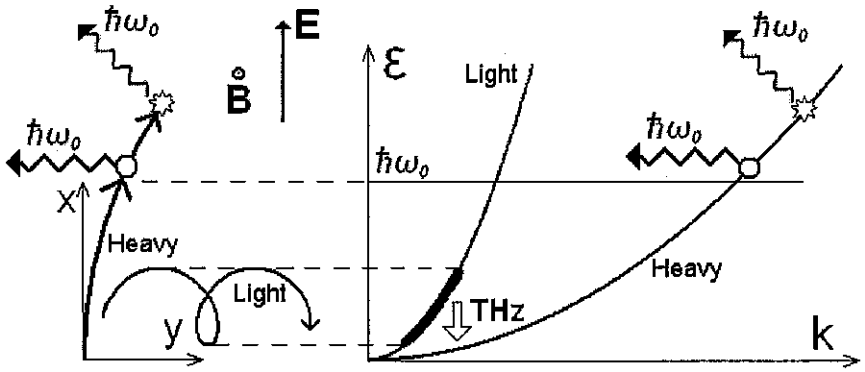

Fig. 1. Schematic of quasi-classical explanation for intersubband hot-hole laser.

We recently developed a terahertz laser concept based on inter-valence-band transitions of holes with transport in crossed electric E and magnetic B fields in a planar periodically doped p-Ge/Ge structure.[5-6] The design, shown schematically in Fig. 2, achieves spatial separation of hole accumulation regions from the doped layers, which reduces ionized-impurity scattering and carrier-carrier scattering for the majority of light holes, allowing significant increase of total carrier concentration without affecting light hole life time. The resulting increase in gain over the bulk p-Ge laser promises to raise maximum operation temperatures to 77 K. At the same time the proposed laser retains the intersubband mechanism with its wide tuning range 1-4 THz. Moreover, this crystalline-Ge device can be grown by chemical vapor deposition (CVD), which allows active thicknesses comparable to the THz wavelength, thus allowing low-loss quasi-optical cavity solutions. As soon as we have developed a THz laser concept based on CVD epitaxial Ge devices, it becomes very interesting to consider the possibility of realizing a similar structure based on GaAs, because of the highly sophisticated technology available for epitaxial growth of this material.

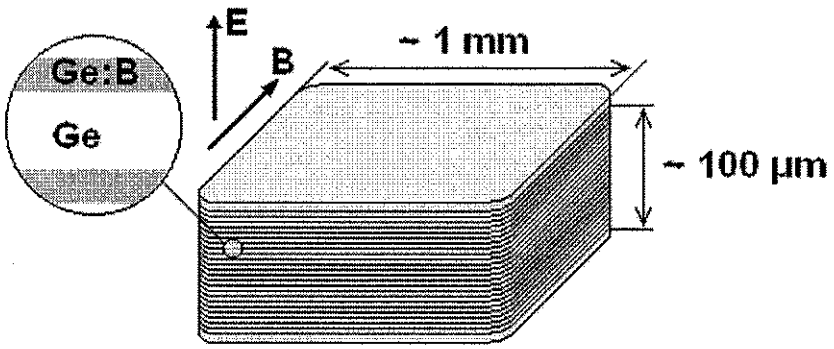

Fig. 2. Homoepitaxial multilayer p-type semiconductor structure THz laser concept for germanium. The layer period is chosen to be 200 –500 nm, which is larger than the light hole cyclotron orbit, but smaller than that for heavy holes. The doped layers are ~10% as thick as the period. Light holes are shown by Monte Carlo simulation to accumulate in the undoped layers where their life time is enhanced by reduced impurity scattering. This scheme allows much higher average carrier concentrations than for uniformily doped bulk, giving a corresponding increase in gain. The stack thickness achievable for germanium by chemical vapor deposition is estimated to be 100 μm. In the case of a GaAs structure, the total stack thickness that can been achieved by vapor phase epitaxy would be up to 800 microns, giving a low-loss quasioptical cavity solution.

2. THEORETICAL METHODS

Hole dynamics, hole distribution functions, and the gain on direct optical light-to-heavy hole transitions in p-GaAs are calculated by the Monte-Carlo simulation method using classical motion equations and hole scattering probabilities.[13-14] Two valence subbands (light and heavy holes) with isotropic and parabolic dispersion laws are considered. The isotropic approach is justified by the relatively small warping of the GaAs valence band. We can neglect quantum confinement effects because the considered structure has no heteroboundaries, only delta-doped layers. We also neglect Landau quantization, which is a good approximation for magnetic fields of 3 – 4 T and below. Time or ensemble averaged momentum and position yield the hole distribution functions $f_{l,h}(\mathbf{k},\mathbf{r})$ (subband (l,h), wavevector **k**, and coordinate **r**). The distribution functions were considered uniform in the horizontal planes according to the geometry of the problem. The standard Rees rejection technique chooses among scattering processes.[13] The rate of each scattering process is given by a temperature-dependent analytic expression. Polar and non-polar optical phonon scattering is treated in a deformation potential approximation.[11] Acoustic phonon scattering is simplified according to Ref. 15. Inelasticity for acoustic phonon scattering is included.[16] Piezoelectric scattering is treated according to Ref. 17. Brooks-Herring model[17] with inverse Debye screening length and Yukawa potential was used for ionized impurity scattering. Hole-hole scattering was calculated according to Ref. 18. Iteration determines the self-consistent solution of the Poisson equation and thereof the spatial carrier distribution and potential profile. The small signal gain is calculated as the difference between the gain on direct inter-valence-band (light to heavy hole) transitions and free carrier absorption assisted by phonons and ionized impurities.[19,20] Up to liquid nitrogen temperatures and impurity concentrations of ~ 10^{15} - 10^{16} cm^{-3}, the main contribution to free carrier absorption in GaAs comes from polar optical phonon emission by heavy holes. Lattice absorption[21] was not included in the calculations.

Strong inter-valence-band (heavy-to-light) polar-optical phonon scattering in p-GaAs populates the light-hole band. In contrast to non-polar optical phonon scattering, most of these scattering events occur right beyond the sharp energy threshold for polar-phonon scattering (see Fig. 1). As a result, after emission of an optical phonon light holes are created with very small kinetic energy. These slow holes experience very strong ionized impurity and hole-hole scattering, which is enhanced in GaAs compared to Ge because of the smaller relative permittivity (ε_r = 12.9 for GaAs vs 16.0 for Ge). These holes are quickly accelerated by the applied electric field, but they return to the low-energy range on each loop of cyclotron trajectory in crossed fields. The ionized impurity scattering is the dominant light-hole-band depopulating mechanism. Similarly, ionized impurity scattering of heavy holes is also stronger in GaAs compared to Ge. Acoustic deformation potential scattering rates in GaAs are similar to rates in Ge. Piezoelectric scattering is weak and can be neglected. In order to maintain an inverted distribution of holes and to reduce the effect of ionized impurity scattering for light holes in GaAs, the magnitude of the applied fields must be higher than typical for the p-Ge laser (E = 1 – 2 kV/cm, B = 1 – 2 T).

3. CALCULATIONS FOR UNIFORMLY DOPED MATERIALS.

For direct comparison of the scattering effects in germanium and GaAs, the distribution functions averaged over directions are plotted in Fig. 3 for both materials in strong crossed electric (E = 4 kV/cm) and magnetic (B = 3 T) fields at T = 20 K for carrier concentration p = 2.5 x 10^{14} cm^{-3}. Note in Fig. 3 the "hard ceiling" for heavy hole energies in the case of GaAs that occurs at the 35 meV optical phonon energy. This effect causes the hole distribution for GaAs to be shifted into low-energy regions compared with Ge.

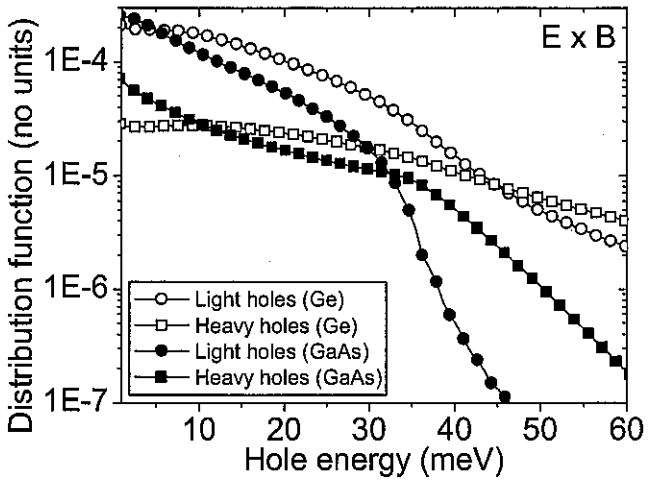

Fig. 3. Calculated distribution functions of light and heavy holes in Ge and GaAs. E = 4 kV/cm, B = 3 T, T = 20 K, and p = 2.5x10^{14} cm^{-3}.

Calculated gain for amplification on direct inter-valence-band transitions, and free-carrier absorption, for bulk p-Ge and p-GaAs are presented in Figs. 4 and 5, respectively. The simulation parameters for Ge (GaAs) were E = 1.5 kV/cm, B = 1.2 T, T = 10K, $p = 10^{14}$ cm^{-3} (E = 4 kV/cm, B = 3.5 T, T = 10K, $p = 2 \times 10^{14}$ cm^{-3}). The total gain is smaller for GaAs than for Ge, despite the much higher applied fields and twice higher hole concentration. Fields need to be increased over those for Ge, in principle, to achieve *any* positive gain in GaAs. One reasons for this is the almost twice smaller oscillator strength for GaAs.[22] A second reason is stronger free carrier absorption, which arises because phonon scattering rates are higher, and this factor is especially unfavorable considering that the inversion between light- and heavy-hole bands is shifted to lower energy in GaAs.

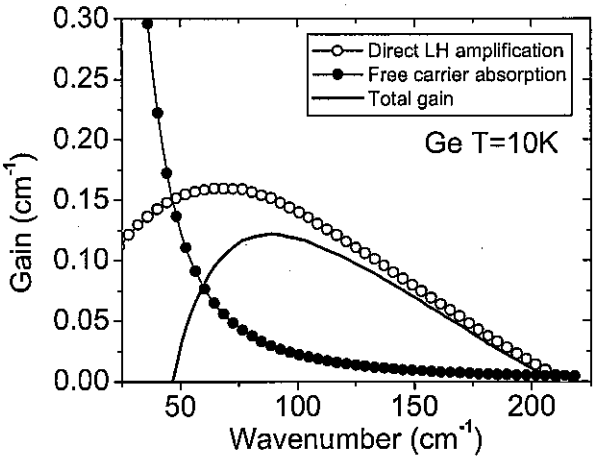

Fig. 4. Calculated inter-valence-band gain and free carrier absorption in bulk p-Ge with carrier concentration 10^{14} cm^{-3}. E = 1.5 kV/cm, B = 1.2 T, T = 10K. Total gain (smooth curve) is the difference between two curves with symbols.

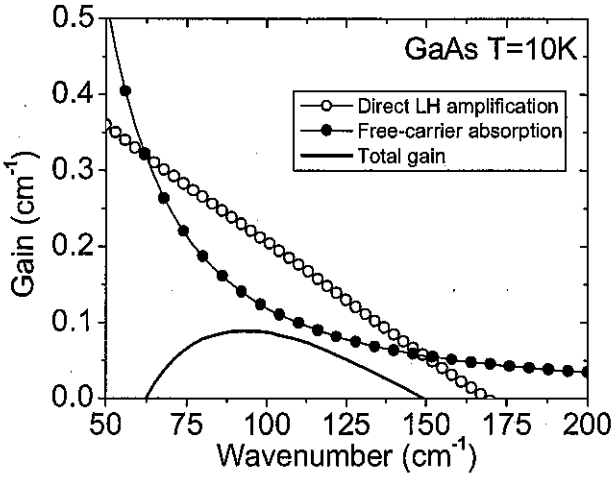

Fig. 5. Calculated inter-valence-band gain and free carrier absorption in bulk p-GaAs with carrier concentration $2x10^{14}$ cm^{-3}. E = 4 kV/cm, B = 3.5 T, and T = 10 K. The total gain (smooth curve) is the difference between two curves with symbols.

The maximum value of the calculated gain in bulk p-GaAs is presented in the contour plot Fig. 6 as a function of the applied fields. The interval between contour plots is 0.025 cm^{-1}. Here and below, the contours are spline-interpolated. The waves in the contours are caused by the interpolation to the limited set of data points, which occur at every grid intersection. As has been shown previously,[10] the optimal ratio of fields and their magnitudes must be different for the two materials, and the gain in GaAs can be increased by applying higher electric (~ 8 kV/cm) and magnetic (~ 7 T) fields. However, the validity of classical approach for Monte Carlo simulation under these extreme conditions becomes questionable. Performance of p-GaAs hot-hole lasers would be improved by the periodic doping scheme, suggested in the introduction, by which impurity scattering is eliminated from the active region. The same device concept with vertical transport, which has been demonstrated theoretically for Ge,[5] can be applied directly to GaAs. This will be discussed next.

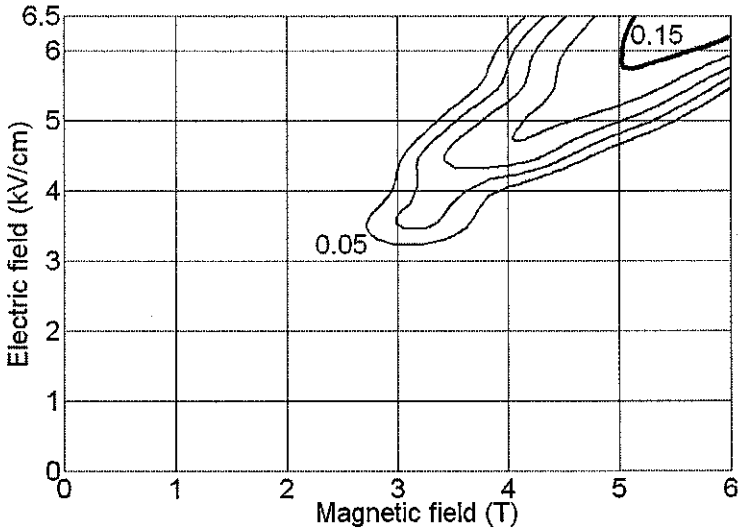

Fig. 6. Gain for uniformly doped p-GaAs as a function of applied fields. Simulation parameters are $p = 2x10^{14}$ cm^{-3}, T = 10 K.

4. CALCULATIONS FOR DELTA DOPED STRUCTURE

A delta doped p-GaAs/GaAs structure, with doping period $d = 200$ nm (20% doped, 80% undoped) and average carrier concentration $2x10^{14}$ cm^{-3}, was used for preliminary gain estimations. The electric and magnetic fields are 4 kV/cm and 3.5 T, respectively, and the lattice temperature is 10 K. Calculated spatial distribution of light and heavy holes across two structure periods is presented in Fig. 7. Heavy holes have a slightly larger concentration near the doped regions. Most of the light holes are concentrated in the undoped region between two doped layers. Because of the much larger density of states of the heavy hole band, the calculated distribution in the undoped regions constitutes a population inversion.

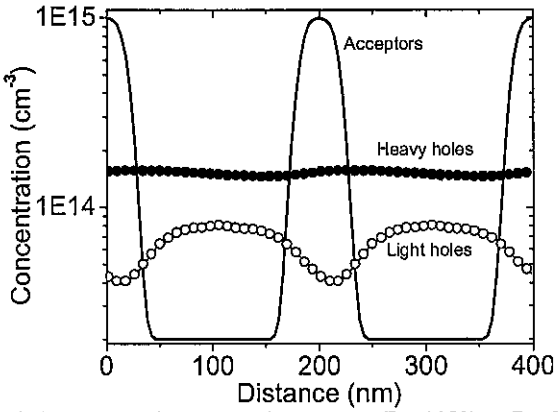

Fig. 7. Distribution of light and heavy hole concentrations across the structure. E = 4 kV/cm, B = 3.5 T, $d = 200$ nm, $p = 2x10^{14}$ cm^{-3}.

The resulting spatial-spectral gain distribution is shown in Fig. 8. Strong inversion is observed in the regions of undoped GaAs. The doped layers are absorbing.

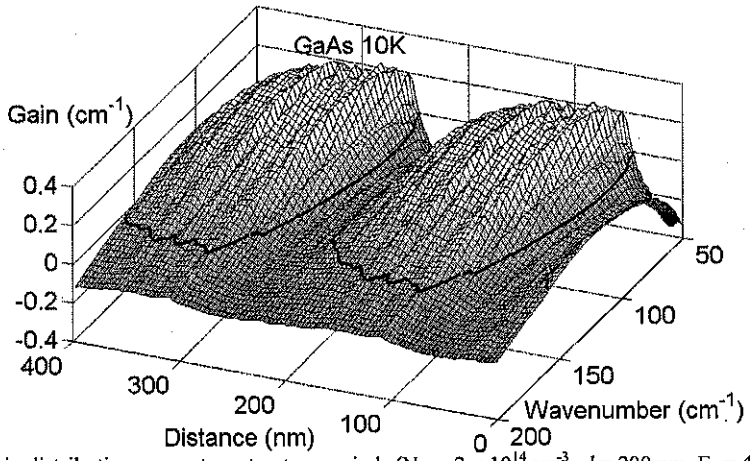

Fig. 8. Spatial-spectral gain distribution across two structure periods ($N_{av} = 2 \times 10^{14}$ cm^{-3}, $d = 200$ nm, E = 4 kV/cm, B = 3.5 T, T = 10 K) with free carrier absorption included.

The spatially averaged net gain in the structure is presented in Fig. 9. Compared to Fig. 5 for bulk p-GaAs the gain is approximately twice higher. The gain spectrum is ~ 50 – 150 cm^{-1} wide, but this will be modified by the lattice absorption (not included in the calculations). Note that all simulation parameters are the same as in Fig. 5 for bulk GaAs (fields, average concentration, temperature) except the doping profile, so that the observed improvement is purely an effect of the selective doping. As will be shown below, an additional improvement of the gain by increase in the carrier concentration, as was observed for p-Ge/Ge structures,[5,6] is not achievable for GaAs.

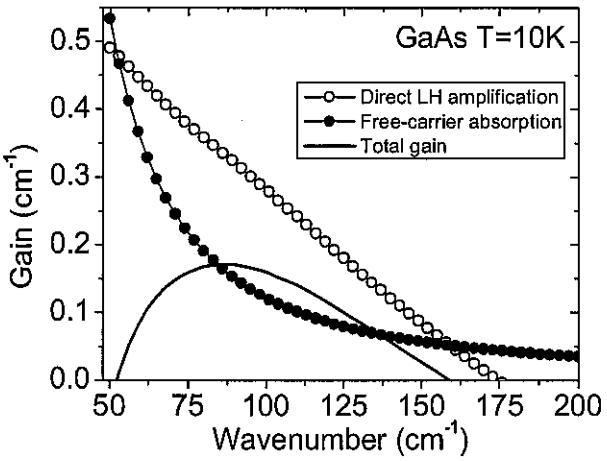

Fig. 9. Calculated spatially-averaged terahertz gain and free carrier absorption in the delta-doped GaAs structure with all other parameters the same as for the uniformly doped case presented in Fig. 5. The total gain (smooth curve) is the difference between two curves with symbols.

Next, we optimize the structure by varying the simulation parameters to maximize the gain. The dependence of peak gain on the magnitude of the applied fields for the structure with fixed doping parameters ($p = 2\text{x}10^{14}$ cm^{-3}, $d = 250$ nm, 10% doped, 90% undoped) is presented in the contour plot Fig. 10. The interval between contours is 0.025 cm^{-1}. Comparison of Figs. 6 and 10 shows that the acceptable range of the applied fields is wider for the delta-doped structure than for the uniformly doped GaAs (see 0.15 cm^{-1} contours in both figures). The gain achievable for delta doped structure is about twice higher than for bulk p-GaAs.

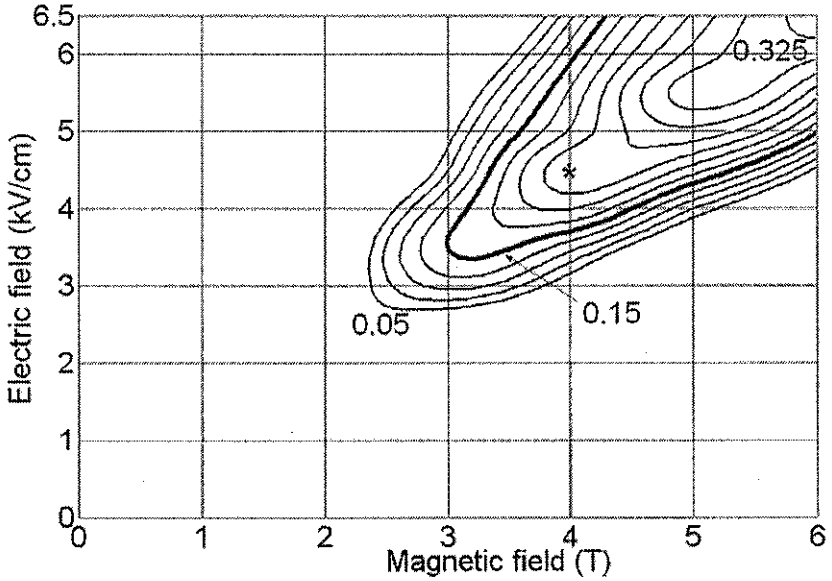

Fig. 10. Gain for delta-doped p-GaAs/GaAs structure as a function of applied fields. Simulation parameters are $p = 2\text{x}10^{14}$ cm^{-3}, $d =$ 250 nm (10% doped, 90% undoped), T = 10 K.

Next, we consider the effect of varying the doping parameters (structure period and average carrier concentration) while holding the applied fields fixed. These fields (E = 4.5 kV/cm, B = 4 T) correspond to the point indicated by an asterisk in Fig. 10. The relative thickness of the p-GaAs doped layers is fixed and equal to 10% of the period as before. The gain surface is shown in Fig. 11 by contours with 0.025 cm^{-1} intervals. In contrast to p-Ge/Ge structures,[5] the optimal average carrier concentration for the delta doped p-GaAs/GaAs structure is comparable to that for uniformly doped p-GaAs[10] and equal to ~2 x 10^{14} – 4 x 10^{14} cm^{-3}. The optimal range of the structure period is 250 – 500 nm for the chosen fields. As can be seen from the Fig. 11, the gain is very sensitive to the structure period at high doping concentrations. This is caused by the distortion of electric potential across the structure period, which changes the ratio of the local electric and magnetic fields and hole lifetime. At low carrier concentration the gain surface does not show such a strong dependence on structure period as soon as the average light hole cyclotron orbit (which decreases with increase in magnetic fields) fits inside the undoped layer (see decrease in the gain in the low period part of the Fig. 11) to provide a long lifetime of the light hole and therefore inversion. The asterisk in Fig. 11 indicates the structure parameters for the calculations in Fig. 10.

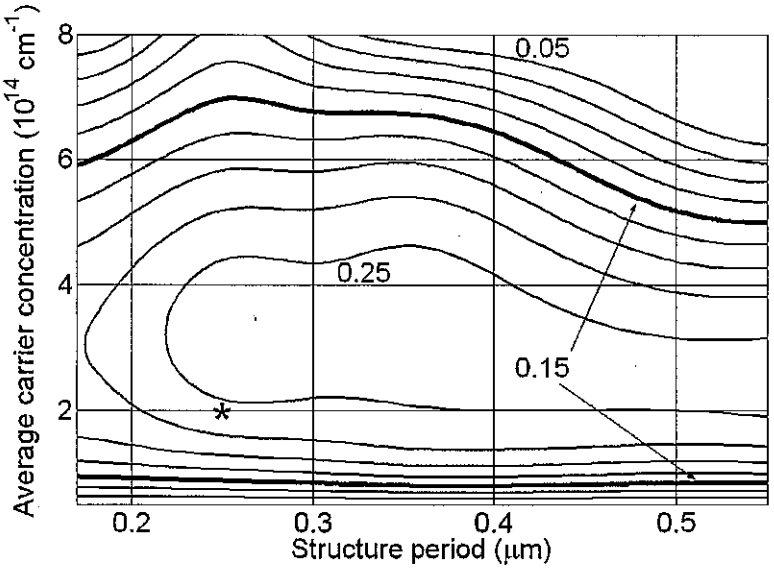

Fig. 11. Gain for p-GaAs/GaAs structure as a function of carrier concentration and structure period. Simulation parameters E = 4.5 kV/cm, B = 4T, T = 10 K. The relative thickness of the doped p-GaAs layers is 10% of the structure period.

5. GROWTH FEASIBILITY

Thick epitaxial GaAs is made possible by hydride vapor phase epitaxy (HVPE), which can achieve much faster growth rates than the more widespread GaAs epitaxial growth methods (molecular beam epitaxy or organometallic vapor phase epitaxy). We have demonstrated growth rates well above 100 μm/hr for homoepitaxial GaAs via HVPE in a custom-built reactor at the Air Force Hanscom Research Site.[23] The system consists of a horizontal quartz tube, heated by a three-zone furnace and sealed to allow low pressure operation in the range of 1 to 5 torr (Fig. 12). HCl vapor passing over a liquid Ga source reacts to form GaCl, which is transported to the substrate. Arsenic is supplied in the form of arsine (AsH_3), which decomposes on the surface. Both the Ga source and the substrate are heated to temperatures in the range of 650 to 750°C; the temperature gradient along the tube drives GaCl formation at the source and GaAs deposition on the substrate. The growth rate can be controlled by varying the vapor supersaturation – i.e., increasing or decreasing the partial pressures of the reactants with respect to their equilibrium values alters the tendency toward growth or etching of GaAs. This control allows us to achieve very rapid epitaxial growth rates, and we regularly achieve thicknesses in the range of 500 to 800 μm in single HVPE runs. The p-type dopant will be introduced through an additional port and mixed with the gases upstream of the wafer. At a growth rate of 100 μm/hr, a doping period of 200 nm corresponds to 8 seconds. Abrupt doping transitions are facilitated in our system by the use of a rapid gas velocity

through the reactor at low pressure, allowing for very short dopant residence times. Therefore, the growth of multilayer delta-doped p-GaAs/GaAs structures of up to 800 μm total thickness is attainable.

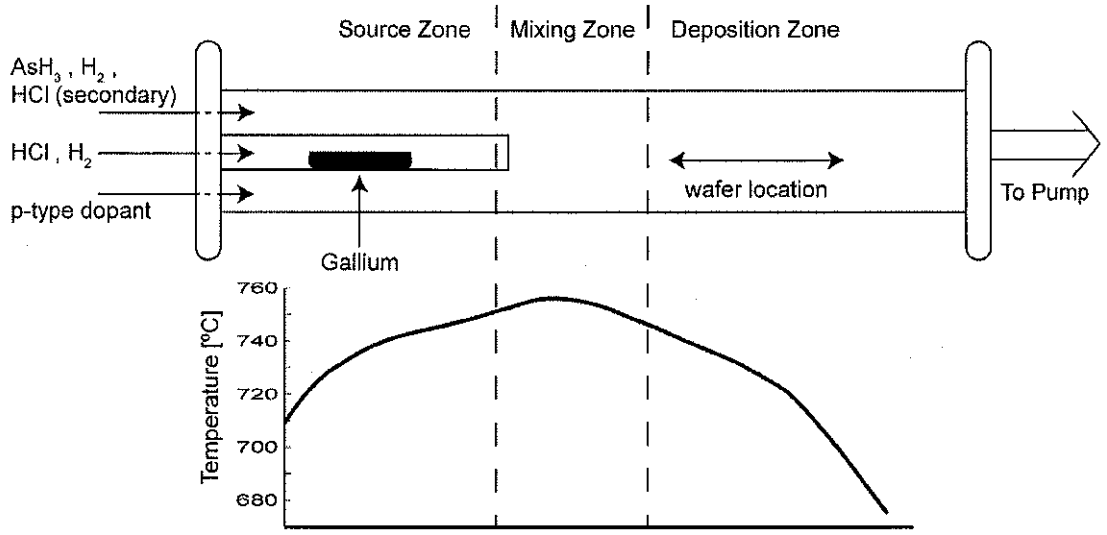

Fig. 12. Schematic of low-pressure hydride vapor phase epitaxial reactor. GaAs growth rates of up to 150 μm/hr and total thicknesses of 800 μm have been demonstrated.

6. SUMMARY

Gain calculations for a delta-doped homoepitaxial p-GaAs/GaAs THz laser structure were performed, and the results were compared with recently published calculations for a similar p-Ge/Ge laser structure. Though the GaAs structure gives lower gain and requires higher applied fields than found for Ge, GaAs has the advantage of the existence of more highly developed epitaxial growth technology. Indeed, consideration of the potential of a particular vapor-phase-epitaxy growth reactor suggests that growth of the considered device structure, with sufficient active thickness for low-loss quasi-optical cavity solutions, is feasible. What remains to be done is experimental demonstration of the growth of the device with comparison of physical, electrical, and optical characterization data to design specifications and comparison with calculations. Expectations are the development of a new type of THz laser technology that can compete favorably with MBE grown quantum cascade lasers.

ACKNOWLEDGMENTS

This work was funded by the Air Force Office of Scientific Research and was initiated during an ASEE/AFOSR Faculty Summer Fellowship for RE Peale at AFRL Hanscom AFB. UCF Authors acknowledge AFRL/SNHC and Dr. Gernot Pomrenke of the AFOSR for support to perform the calculations presented here.

REFERENCES

1. A. Maestrini, J. Ward, J. Gill, H. Javadi, E. Schlecht, G. Chattopadhyay, F. Maiwald, N. R. Erickson, and I. Mehdi "A 1.7-1.9THz Local Oscillator Source," IEEE Microwave and Wireless Components Lett. 4, 253-255 (2004).
2. R. Kohler, A. Tredicucci, F. Beltram, H. E. Beere, E. H. Linfield, A. G. Davies, D. A. Ritchie, S. S. Dhillon, and C. Sartori," High-performance continuous-wave operation of superlattice terahertz quantum-cascade lasers" Appl. Phys. Lett. **82**, 1518-1520 (2003).
3. K. L. Vodopyanov, G. Imeshev, M. E. Fermann, J. Schaar, M. M. Fejer, X. Yu, J. S. Harris, D. Bliss, and D. Weyburne "Tunable 0.8-3.5THz Source based on Fiber-laser Pumped Orientation-patterned GaAs" to be presented at CLEO, Long Beach CA, May 21, 2006.

4. L. A. Eyres, P. J. Tourreau, T. J. Pinguet, C. B. Ebert, J. S. Harris, M. M. Fejer, L. Becouarn, B. Gerard, and E. Lallier, "All-epitaxial fabrication of thick, orientation-patterned GaAs films for non-linear optical frequency conversion," Appl. Phys. Lett. **79**, 904-906 (2001).
5. M. V. Dolguikh, A.V. Muravjov, R. E. Peale, M. Klimov, O. A. Kuznetsov, E. A. Uskova, "Terahertz gain on intersubband transitions in multilayer delta-doped p-Ge structures," J. Appl. Phys. **98**, 023107 (2005).
6. M. V. Dolguikh, A. V. Muravjov, R. E. Peale, "Terahertz amplification in delta-doped germanium films with in-plane transport," J. Appl. Phys. **99**, no. 8 (15 Apr 2006), in press.
7. E. Bründermann, "Widely Tunable Far-Infrared Hot-Hole Semiconductor Lasers" in *Long wavelength infrared semiconductor lasers*, edited by H. K. Choi, pp. 279-343, Wiley, NJ, 2004.
8. V. N. Shastin, "Hot hole inter-sub-band transition p-Ge FIR laser", Opt. Quantum Electron. **23**, S111-131 (1991).
9. A. A. Andronov, A. M. Belyantsev, E. P. Dodin, V. I. Gavrilenko, Yu. L. Ivanov, V. A. Kozlov, Z. A. Krasil'nik, L. S. Mazov, A. V. Muravjov, I. M. Nefedov, V. V. Nikanorov, Yu. N. Nozdrin, S. A. Pavlov, V. N. Shastin, V. A. Valov, and Yu. B. Vasil'ev, "Tunable hot hole FIR lasers and CR masers", Physica B **134**, 210 (1985).
10. P. Kinsler and W. Th. Wenckebach, "Hot-hole lasers in III-V semiconductors", J. Appl. Phys. **90**, 1692-1697 (2001).
11. T. Brudevoll, T. A. Fjeldly, J. Baek, and M. S. Shur, "Scattering rates for holes near the valence-band edge in semiconductors," J. Appl. Phys. **67**, 7373-7382 (1990).
12. M. Neuberger, *Handbook of Electronic Materials*, *vol. 2*, Plenum, New York, 1971.
13. C. Jacoboni and L. Reggiani, "The Monte Carlo method for the solution of charge transport in semiconductors with applications of covalent materials," Rev. Mod. Phys. **55**, 645 (1983).
14. C. Jacoboni, R. Brunetti, and P. Bordone, "Monte Carlo simulation of semiconductor transport," in *Theory of Transport Properties of Semiconductor Nanostructures*, edited by Eckehard Scholl, p. 59, Chapman & Hall, London, 1998.
15. J. D. Wiley, "Polar mobility of holes in II-V compounds," Phys. Rev. B **4**, 2485-2493 (1970).
16. E. V. Starikov, P. N. Shiktorov, "Numerical simulation of far infrared emission under population inversion of hot sub-bands", Optical and Quantum Electronics, **23**, S177-193, (1991).
17. B. K. Ridley, *Quantum Processes in Semiconductors*, Oxford, NY, 1999.
18. M. V. Dolguikh, A. V. Muravjov, and R. E. Peale, "Intervalenceband hole-hole scattering in cubic semiconductors," Phys. Rev. B **73**, 075327 (2006).
19. Yu. K. Pozhela, E. V. Starikov, and P. N. Shiktorov, "Far infrared absorption by hot holes in p-Ge under $E \perp B$ fields," Phys. Stat. Sol. (b) **128**, 653 (1985).
20. M. V. Dolguikh, *Monte Carlo simulation of hole transport and terahertz amplification in multilayer delta doped semiconductor structures*, PhD dissertation, University of Central Florida, Orlando FL 2005.
21. R. Brazis and F. Keilmann, "Lattice absorption of Ge in the far infrared," Solid State Comm. **70**, 1109 (1989).
22. M. V. Dolguikh, A.V. Muravjov, R. E. Peale, R. A. Soref, D. Bliss, C. Lynch, and D. W. Weyburne, "Toward hot-hole THz lasers in homoepitaxial Si and GaAs with layered doping," in *Nanoengineering: Fabrication, Properties, Optics, and Devices II*, edited by E. A. Dobisz and L. A. Eldada, Proc. SPIE **5931**, 310 (2005).
23. D. Bliss, C. Lynch, D. Weyburne, K. O'Hearn, and J. Bailey, "Epitaxial Growth of Thick GaAs on a Patterned Wafer for NLO Applications," J. Crystal Growth **287**, 673 (2006).